SIRT1 Is an Actionable Target to Restore p53 Function in HPV-Associated Cancer Therapy

Irene Lo Cigno[1], Federica Calati[1], Carlo Girone[1], Cinzia Borgogna[1], Aldo Venuti[2], Renzo Boldorini[3], Marisa Gariglio[1*]

[1] Virology Unit, Department of Translational Medicine, Eastern Piedmont University, Novara, Italy.

[2] HPV Unit, UOSD Tumor Immunology and Immunotherapy, IRCCS Regina Elena National Cancer Institute, Rome, Italy.

[3] Pathology Unit, Department of Health Sciences, Eastern Piedmont University, Novara, Italy.

* Corresponding author

Marisa Gariglio

Virology Unit, Department of Translational Medicine

Eastern Piedmont University, Novara, 28100, Italy

Phone: +39 0321 660649

ORCID ID: https://orcid.org/0000-0002-5187-0140

Email: marisa.gariglio@med.uniupo.it (MG)

ABSTRACT

BACKGROUND: Our aim was to evaluate the efficacy and anti-cancer action of a precision medicine approach involving a novel SIRT1-dependent pathway that, when disrupted, leads to the restoration of a functional p53 in human papillomavirus (HPV)-transformed cells.

METHODS: The anticancer potential of inhibiting SIRT1 was evaluated by examining the effects of the specific SIRT1 inhibitor EX527 (also known as Selisistat) or genetic silencing, either individually or in conjunction with standard chemotherapeutic agents, on a range of HPV^+ cancer cells and a preclinical mouse model of HPV16-induced cancer**.**

RESULTS: We show that SIRT1 inhibition restores a transcriptionally active K382-acetylated p53 in HPV^+ but not HPV^- cell lines, which in turn promotes G_0/G_1 cell cycle arrest, and inhibits clonogenicity specifically in HPV^+ cells. Additionally, EX527 treatment increases the sensitivity of HPV^+ cells to sublethal doses of standard genotoxic agents. The enhanced sensitivity to cisplatin as well as p53 restoration were also observed in an *in vivo* tumorigenicity assay using syngeneic C3.43 cells harboring an integrated HPV16 genome, injected subcutaneously into C57BL/6J mice.

CONCLUSIONS: Our findings uncover an essential role of SIRT1 in HPV-driven oncogenesis, which may have direct translational implications for the treatment of this type of cancer.

BACKGROUND

High-risk human papillomaviruses (hrHPVs) from the α genus are responsible for the development of squamous cell carcinoma (SCC) of the anogenital and upper aerodigestive tract, with an incidence of ~5% among all cancers worldwide [1-4].

In the last two decades, mounting evidence has shown that HPV16 and, with less frequency, HPV18 are etiologically involved in a subset of head and neck cancers (HNCs), namely oropharyngeal squamous cell carcinomas (OPSCCs). While virtually all cervical cancers are HPV-driven, the fraction of OPSCCs likely arising from HPV infection—mainly HPV16—has been estimated to be ~20% [2-6]. In this regard, the most recent edition of the American Joint Committee on Cancer (AJCC) staging system has clearly defined HPV^+ and HPV^- OPSCCs as separate entities, with distinct molecular profiles, tumor characteristics and outcomes. In particular, HPV^+ OPSCC is predominantly found in young white people and is associated with a more favorable prognosis compared to HPV^- OPSCC [2, 7]. However, the high cure rates often come to the expense of severe long-term adverse effects due to not only the devastating impact of radiotherapy or surgery on the targeted anatomical sites but also the cytotoxic side effects of the adjuvant therapies [6]. Thus, there is a critical clinical need for alternative strategies that may allow de-escalating current drug therapies to optimize oncologic outcomes while reducing treatment-related acute and long-term toxicities [8-10].

The development and maintenance of HPV-associated cancers relies on the expression of two oncoproteins, E6 and E7, which interact with host cell factors to create an environment conducive to cellular transformation [11-13]. Specifically, hrHPV E6 binds to and promotes degradation of the tumor suppressor protein p53, triggering uncontrolled cell proliferation through cell cycle checkpoint evasion, whereas hrHPV E7 binds to the tumor suppressor protein and major G_1 checkpoint regulator pRb to induce S phase entry. Thus, the very distinctive trait of this type of cancer is that HPV^+ cancer cells retain unaltered p53 and pRb genes, unlike most human tumors that harbor mutations in these tumor suppressor genes [13-16].

Sirtuins are an evolutionarily conserved family of NAD^+-dependent deacetylases and ADP-ribosyltransferases that play important roles in a broad range of biological activities.

SIRT1, the principal NAD^+-dependent deacetylase in mammalian cells, catalyzes the deacetylation of its substrates, which include histone and non-histone targets, such as p53 [17-23]. A series of reports have already demonstrated that SIRT1 is a critical regulator of multiple aspects of high-risk HPV life cycle, encompassing transcription and replication during the differentiation-dependent phase. Specifically, SIRT1 has been shown to bind to the HPV31 genome and regulate both viral chromatin remodeling as well as viral DNA binding of members of the homologous repair pathway. This activity is necessary for both histone deacetylation and recruitment of DNA damage repair factors, which are critical steps during the HPV life cycle [24]. SIRT1 was also reported to be part of the E1-E2 DNA replication complex and is recruited to the HPV viral origin of replication in an E1-E2-dependent manner [25]. In addition, it is strongly upregulated in HPV^+ cells and cervical intraepithelial neoplasia (CIN) in an E7-dependent fashion, with an increasing trend from low-to high-grade CIN1 to 3 [26, 27]. Although SIRT1-mediated regulation of p53 stability is well known—p53 acetylation at K382 competes with ubiquitination and promotes p53 stabilization and activation—its engagement in E6/E7-driven oncogenesis has never been explored [22, 23, 28-32]. The current consensus is that, in HPV-transformed cells, p53 levels are kept very low by the cellular ubiquitin ligase E6AP. In this process, E6 binds to a short LxxLL consensus sequence within E6AP, forming an E6/E6AP heterodimer that recruits and degrades p53. The E6/E6AP/p53 complex is thus regarded as a prototype of viral hijacking of both ubiquitin-mediated protein degradation and p53 tumor suppressor activity [13-16, 33]. Whether SIRT1 interacts or cooperates with this molecular platform is currently unknown.

In this study, we demonstrate that in addition to the canonical E6AP pathway, another cellular mechanism involving SIRT1-dependent p53 deacetylation contributes to p53 inhibition in HPV-driven oncogenesis whose disruption leads to restoration of a functional p53

in HPV-transformed cells. Lastly, we demonstrate that SIRT1 inhibition increases tumor cell sensitivity to sublethal doses of genotoxic agents, such as doxorubicin (DX) or cisplatin (Cis).

Altogether, our findings uncover an essential role of SIRT1 in HPV-associated cancers and provide compelling evidence that pharmacological inhibition of SIRT1 may allow treatment de-intensification strategies for this type of cancer.

MATERIALS AND METHODS

Cell culture, plasmids, transfection, and treatments

HeLa (CRM-CCL-2™-ATCC, Manassas, VA, USA), C33A (HPV^- cervical carcinoma-derived cell line, HTB-31™-ATCC, RRID:CVCL_1094), and HNO150 (HPV^- laryngeal squamous cell carcinoma cell line, kindly provided by Massimo Tommasino-Italy), were grown in DMEM (Sigma-Aldrich, St. Louis, MO, USA). CaSki (CRM-CRL-1550™-ATCC) and C3.43 cells, kindly provided by Martin Kast (USA), were grown in RPMI (Thermo Fisher Scientific, Waltham, MA, USA) supplemented with 10% FBS (Sigma-Aldrich) [34-36]. NOKsHPV16E6/E7 (for brevity: NOKE6/E7) are normal oral keratinocytes stably transduced with both E6 and E7 genes from HPV16 by lentiviral infection that were kindly provided by Frank Rösl (Germany) and were cultured as previously described [37]. A highly expressing E6 and E7 clone with high proliferation rates was isolated from a pool of NOKE6/E7 cells by limiting dilution. Cells derived from this clone were used for all experiments between passage 10 and 20. The HPV16-positive hypopharyngeal squamous cell carcinoma cell line SCC152 was purchased from ATCC (ATCC-CRL-3240, RRID:CVCL_C058) and cultured in minimum essential medium Eagle (EMEM; ATCC), supplemented with 10% fetal bovine serum (FBS; Thermo Fisher Scientific), 2 mM L-glutamine (Gibco, Thermo Fisher Scientific), MEM non-essential amino acid solution (NEAA; Gibco, Thermo Fisher), and 50 µg/mL gentamicin (Gibco, Thermo Fisher Scientific). Cells were treated with EX527 (6-chloro-2,3,4,9-

tetrahydro-1H-carbazole-1-carboxamide, also known as Selisistat) (80 μM) (Sigma-Aldrich), DX (1.5 μM for HeLa, NOKE6/E7, SCC152, C33A, and HNO150 or 0.5 μM for CaSki) (Cayman Chemical Company, Ann Arbor, MI, USA) or Cis (10 μM for HeLa, 15 μM for CaSki, C33A, and HNO150, 2.5 μM for NOKE6/E7, and 5 μM for SCC152) (Sandoz, Basel, Switzerland).

Cells were transfected with siRNA against SIRT1 (L-003540-00-0005, ON-TARGETplus SMARTpool siRNA; Dharmacon, Lafayette, CO, USA), p53 (M-003329-03-0005, siGENOME SMARTpool siRNA; Dharmacon), E6E7 HPV18 (forward GCUAGUAGUAGAAAGCUCA, reverse UGAGCUUUCUACUACUAGC; Sigma-Aldrich), E6E7 HPV16 (forward GACAGAGCCCAUUACAAUA, reverse UAUUGUAAUGGGCUCUGUC; Sigma-Aldrich), or control siRNA (D-001206-13-05, siGENOME non-Targeting siRNA Pool; Dharmacon) using Lipofectamine RNAiMax transfection reagent (Invitrogen, Thermo Fisher Scientific).

Immunohistochemistry

Consecutive 5-μm-thick sections obtained from formalin-fixed and paraffin-embedded tissues were processed for immunohistochemical detection of antigens. Antigen unmasking was performed by heating the slides in a conventional decloaking chamber at 750W for 15 min, followed by an additional step at 350W for 10 min in 10 mM citrate buffer at pH 6.0 (Vector Laboratories, Burlingame, CA, USA). Primary antibodies were diluted in 5% normal goat serum/PBS and incubated ON at 4°C. The following Abs were used: anti-p53 (MA5-15244; RRID:AB_10981260, Thermo Fisher Scientific, diluted 1:1000), and anti-Ki67 (ab16667; RRID:AB_302459, Abcam (Cambridge, UK), diluted 1:200). For the assessment of histological features, the slides analyzed were stained with hematoxylin and eosin (H&E). Tissue images were acquired using a digital scanner (Pannoramic MIDI; 3DHISTECH,

Budapest, Hungary), and the staining was quantified using QuPath software. For $p16^{INK4a}$, the tumor was considered positive when > 20% of the tumor cells were stained, for p53 the cut-off was > 5%, while for SIRT1 it was > 20%.

Immunoblotting

Whole-cell protein extracts (15 μg) were prepared, transferred to nitrocellulose membrane and subjected to immunoblot as previously described [38].

The following antibodies were used: rabbit polyclonal antibodies anti-Acetyl-p53 (K382) (#2525; RRID:AB_330083, Cell Signaling Technology (Danvers, MA, USA), diluted 1:800), anti-Ac-p53 (K305) (ab109396; RRID:AB_10861725, Abcam, diluted 1:5000), anti-HPV18E6 (GTX132687; RRID:AB_2886711, GeneTex (Irvine, CA, USA), diluted 1:250), anti-HPV18E7 (GTX133412; RRID:AB_2886972, GeneTex, diluted 1:500), anti-HPV16E6 (GTX132686; RRID:AB_2886710, GeneTex, diluted 1:500), and anti-HPV16E7 (GTX133411; RRID:AB_2886971, GeneTex, diluted 1:500) or mouse monoclonal antibodies (MAb) anti-SIRT1 (ab110304; RRID:AB_10864359, Abcam, diluted 1:1000), anti-p53 (sc-126; RRID:AB_628082, Santa Cruz Biotechnology (Dallas, TX, USA), diluted 1:250), anti-$p21^{CDKN1A}$ (P1484; RRID:AB_260888, Sigma-Aldrich, diluted 1:500), anti-$p16^{INK4a}$ (sc56330; RRID:AB_785018, Santa Cruz Biotechnology, diluted 1:500). MAb against α-GAPDH (60004-1-Ig; RRID:AB_2107436, Proteintech (Rosemont, IL, USA) , diluted 1:10000) were used as a control for protein loading. Immunocomplexes were detected using sheep anti-mouse (NA931; RRID:AB_772210, GE Healthcare, Chicago, IL, USA) or donkey anti-rabbit (A6154; RRID:AB_258284, Sigma-Aldrich) immunoglobulin antibodies conjugated to horseradish peroxidase (HRP) and visualized by enhanced chemiluminescence (34580; Super Signal West Pico; Thermo Fisher Scientific) using the instrument ChemiDoc Touch Imaging System (Bio-Rad, Hercules, CA, USA).

ChIP assay

ChIP assay was performed as previously described [39]. The suitability of each antibody for the chromatin immunoprecipitation (ChIP) assay was confirmed by immunoprecipitation-Western blotting (data not shown). Immunoprecipitation was performed with 3 μg of unmodified histone H3 (06-755; RRID:AB_2118461, Merck Millipore, Burlington, MA, USA), acetyl-histone H3 (K9) (07-352; RRID:AB_310544, Merck Millipore), p53 (sc-126; RRID:AB_628082, Santa Cruz Biotechnology), and anti-Ac-p53 (K382) (#2525; RRID:AB_330083, Cell Signaling Technology) antibodies. Threshold cycle (CT) values for the samples were equated to input CT values to provide percentages of input for comparison, and these were normalized to the enrichment level of unmodified histone H3 for each cell line. The following primers were used: p21^{CDKN1A} promoter forward GAGTCTTGCTCAGTGGGAGCTCTGGGAGTA and reverse ATGTGACTTGGGGTGAGGCCTACTCGG; GAPDH promoter forward TTCGACAGTCAGCCGCATCTTCTT and reverse CAGGCGCCCAATACGACCAAATC.

Cell viability assay

Cell viability was determined by 3-(4,5-dimethylthiazol-2-yl)-2,5-diphenyltetrazolium bromide (MTT) (Sigma-Aldrich), as previously described [40].

Flow cytometry analysis

The DNA content and cell cycle phase distribution of cells were evaluated by flow cytometry. Subconfluent cells were serum-starved for 24 h, treated with EX527 for 48 h or transfected with sip53 for 72 h, and then treated with vehicle or EX527 for the last 48 h. Next, cells were harvested, fixed in 70% ethanol at -20°C for 1 h, washed with PBS, resuspended in

a buffer [trisodium citrate (3.4 mM), NaCl (9.65 mM), and 0.003% of NP40] supplemented with RNase (500 µg/mL) and propidium iodide (PI) (20 µg/mL), and then incubated for 15 min at 37˚C in the dark. Cell cycle phase distribution of nuclear DNA was analyzed by Attune™ NxT Flow Cytometer (Thermo Fisher Scientific) using FlowJo software (RRID:SCR_008520).

Clonogenicity assay

A total of 1.5 x 10^3 (HeLa, CaSki, and NOKE6/E7) or 3 x 10^3 (C33A and HNO150) cells were plated in 6-well plates in triplicate and cultured for 15 days. Media supplemented with EX527 (80 µM) was changed every 3 days. Colonies were fixed, stained with 0.1% crystal violet, scanned, and counted with Celigo S Image Cytometer (Nexcelom Bioscience, Lawrence, MA, USA).

Senescence-associated beta-galactosidase activity (SA-β-gal)

For SA-β-gal detection, 3 x 10^4 HeLa, 3.5 x 10^4 CaSki, and 4 x 10^4 NOKE6/E7 were seeded in 6-well plates. At 48, 72, and 96 h post EX527 treatment or 72 h and 96 h post siCtrl, siE6E7, or siSIRT1 transfection, cells were washed in PBS and then fixed for 4 min at RT with 0.3 mL of fixative solution (2% formaldehyde, 0.2% glutaraldehyde diluted in PBS). Fixed cells were washed twice with PBS and then incubated overnight at 37°C in 2 mL of staining solution, without providing CO_2. The staining solution was prepared in deionized water with 1 mg/mL of 5-bromo-4-chloro-3-indolyl-beta-d-galactopyranoside (X-gal, Invitrogen, Eugene, CA, USA), 1× citric acid/sodium phosphate buffer, 5 mM potassium ferricyanide, 5 mM potassium ferrocyanide, 150 mM NaCl and 2 mM $MgCl_2$ [41]. Next, cells were washed twice with PBS and counterstained with 4′,6-diamidino-2-phenylindole (DAPI). Images were acquired using Cytation 5 Cell Imaging Multi-Mode Reader (BioTek, Winooski, VT, USA) in both the DAPI and bright-field channels to visualize nuclei and senescent cells. The raw images

(2×2 montage) were acquired using 4X objective for cell counting, processed, and stitched using the default setting.

Annexin V analysis

To distinguish the types of cell death, double staining for exposed phosphatidylserine and PI exclusion was performed using the Annexin V-FITC Kit (640914; BioLegend, San Diego, CA, USA), according to the manufacturer's instructions. Briefly, cells were plated into 6-well plates (3 x 10^5 cells/well) and treated with EX527 alone or in combination with DX or Cis. After 48 h of treatment, cells were resuspended in Annexin V/FITC and PI buffer and then analyzed by Attune™ NxT Flow Cytometer using FlowJo software (RRID:SCR_008520). Controls of unstained cells, cells stained with Annexin V-FITC only, and cells stained with PI only were used to establish compensation and quadrants. Cells were gated according to their light-scatter properties to exclude cell debris.

***In vivo* tumorigenicity assay**

C57BL/6J mice were housed under pathogen-free conditions in our animal facilities in accordance with "The Guide for the Care and Use of Laboratory Animals", and the experimentation was approved by the Italian Ministry of Health (Agreement No. 219/2020-PR). Five-week-old (female and male) mice were subcutaneously inoculated with 1 x 10^6 C3.43 cells into the back. After 7 days from the inoculum, EX527 (10 mg/kg) alone or in combination with Cis (0.5, 1, 2.5 mg/kg) were injected intraperitoneally every two days for two weeks. Control mice received vehicle alone or in combination with cisplatin. Mice were allocated to experimental groups in a manner ensuring consistent average starting volume across the groups. Mice were daily monitored, tumor growth was measured using a Vernier caliper overtime by a technician blinded to treatment allocation, and the tumor was removed

after two weeks of treatment. Tumor volume was calculated as L x W2/2, where length (L) is the longest dimension and width (W) is the shortest dimension. Tumor weight was also measured.

Statistical analysis

The number of biological replicates per experiment is stated in the figure legends. All statistical tests were performed using Graph-Pad Prism version 8.00 for Windows (GraphPad Software, RRID:SCR_002798). The data are presented as mean ± standard deviation (SD). For comparisons of two groups, means were compared using two tailed Student's t tests. Differences were considered statistically significant at a P value of < 0.05.

RESULTS

Inhibition of SIRT1 activity in HPV$^+$ cancer cells restores a functional Ac-p53 (K382)

As SIRT1 expression has been found to be overexpressed in HPV-induced anogenital cancer, we first asked whether it would be similarly overexpressed in HNC [26, 27]. To this end, we analyzed both SIRT1 mutations and mRNA expression levels using an HNC database from The Cancer Genome Atlas (TCGA) downloaded from the cBioPortal website (https://www.cbioportal.org/) [42]. Whole-exome sequencing data identified 2 amplifications and one in-frame mutation, suggesting that SIRT1 is rarely mutated in HNSCC (1.1%; 3/279 samples) (Fig. 1a). By contrast, the *TP53* gene was found to be mutated in 74% of HPV$^-$ cancers but never in the HPV$^+$ subgroup. We also analyzed SIRT1 mRNA expression in the same dataset by assessing HPV$^+$ *vs* HPV$^-$ cancers and found that SIRT1 mRNA levels were significantly higher in HPV$^+$ than those observed in HPV$^-$ HNCs (Fig. 1b, $P < 0.001$).

As SIRT1 is involved in the regulation of p53 function via deacetylation of its C-terminal Lys382 residue and given that p53 is degraded through E6AP-mediated ubiquitination

in HPV-transformed cells, we next asked whether SIRT1 inhibition could affect p53 stabilization in HPV^+ cells [22, 23, 28-33]. For these experiments, we employed the SIRT1-specific functional inhibitor EX527 at the dose of 80 μM, which had been previously shown to inhibit HPV genome amplification upon differentiation [24, 43]. In addition to the cervical carcinoma-derived cell line HeLa and CaSki—harboring integrated HPV18 and HPV16 genome, respectively—, we also analyzed the NOKsHPV16E6/E7 cell line (hereafter referred to, for brevity, as NOKE6/E7), a newly established model of HPV-induced HN carcinogenesis, where the vector used for lentiviral transduction of normal oral keratinocytes reduces the splicing events and ensures equal expression of E6 and E7 from HPV16 [37, 44]. As shown in Fig. 2a and 2b, pharmacological inhibition of SIRT1 by EX527 led to p53 restoration in all the aforementioned cell lines, whereas no changes in total p53 expression levels were observed in two p53-mutated HPV^- cell lines either derived from genital (C33A) or head and neck cancer (HNO150), indicating that SIRT1 inhibition only influences p53 turnover in HPV^+ cells in which p53 is not mutated but rather degraded through the E6AP ubiquitination pathway [33, 45-48]. Consistent with the notion that the main SIRT1 target site in the p53 protein is K382, expression levels of acetylated p53 [Ac-p53 (K382)] increased significantly in both HPV^+ and HPV^- cell lines following SIRT1 inhibition, albeit to different extents (Fig. 2a and 2b). Notably, quantitation of the ratio between Ac-p53 (K382) levels relative to total p53 showed no variation in HPV^+ cells, indicating that the majority of the restored p53 was K382-acetylated, while this ratio significantly increased in HPV^- cells (Fig. 2c). The latter observation relies on the fact that the total expression levels of mutated p53 in HPV^- cells are not modified upon SIRT1 inhibition despite the enhanced acetylation status of the K382 residue. By contrast, the expression levels of Ac-p53 (K305) were very faint, almost undetectable, in HPV^+ cells even upon SIRT1 inhibition, whereas its expression levels were enhanced by EX527 treatment in HPV^- cell lines (Fig. 2a).

To assess p53 transcriptional activity, we analyzed the expression levels of the downstream target gene $p21^{CDKN1A}$ and found that they were significantly upregulated upon SIRT1 inhibition in HPV^{+} but not HPV^{-} cell lines (Fig. 2a and 2b) [28]. Kinetic experiments in vehicle-treated NOKE6/E7 ruled out that the observed changes in p53 and $p21^{CDKN1A}$ expression levels could be attributed to circadian fluctuations (Supplementary Fig. S1). Consistent with a negative impact of SIRT1 inhibition on E6/E7-induced transformation, the expression levels of $p16^{INK4A}$ decreased over time upon EX527 treatment. No evidence of $p16^{INK4A}$ expression was found in NOKE6/E7, as previously reported [49]. Notably, pharmacological inhibition of SIRT1 led to a robust downregulation of E6 and E7 protein expression in all HPV^{+} cell lines, which was particularly evident in NOKE6/E7 cells, whose basal expression levels of these two oncoproteins were much higher than those observed in CaSki and HeLa cells.

To rule out any unspecific effects due to drug treatment, we inhibited SIRT1 expression in HPV^{+} cells by RNA interference. Consistent with our previous results obtained with EX527 treatment, SIRT1 silencing restored total levels of p53 and $p21^{CDKN1A}$ in all three cell lines (Fig. 2d and 2e). Fittingly, SIRT1 silencing led to increased Ac-p53 (K382) expression, especially in CaSki and NOKE6/E7, while Ac-p53 (K305) remained almost undetectable. Quantitation of Ac-p53 (K382) levels relative to total p53 showed no variation in HPV^{+} cells as already reported upon EX527 treatment (Fig. 2f). Next, we performed chromatin immunoprecipitation (ChIP) assay to assess whether p53 enrichment on the $p21^{CDKN1A}$ promoter region was indeed occurring in response to SIRT1 inhibition. As shown in Fig. 2g, EX527 treatment significantly enhanced the binding of both p53 and Ac-p53 (K382) to the $p21^{CDKN1A}$ promoter region in all the three HPV^{+} cell lines analyzed. By contrast, no significant p53 enrichment was observed when the promoter region of the housekeeping gene glyceraldehyde-3-phosphate dehydrogenase (GAPDH) was amplified. A significant

enrichment of histone H3 lysine 9 acetylated (H3K9Ac) on the $p21^{CDKN1A}$ promoter was also observed in EX527-treated cells because of deacetylase inhibition promoting a switch from inactive heterochromatin into more active open euchromatin conformation, as previously published [17, 50].

Altogether, our findings indicate that the cellular circuit involving SIRT1-dependent p53 deacetylation does contribute to p53 curbing in HPV-driven carcinogenesis, and that its inhibition rescues a transcriptionally active Ac-p53 (K382).

Restoration of Ac-p53 (K382) protein expression suppresses the growth of HPV^+ cells

As p53 inhibition in HPV-driven cancer is crucial to maintain the transforming phenotype and assuming that its reactivation would quickly boost cell cycle arrest due to the intrinsic genomic instability of cancer cells, we assessed the impact of SIRT1 inhibition on cell growth and survival of HPV^+ *vs* HPV^- cells [11, 13-16]. Using a short-term cell proliferation assay, we observed that EX527 treatment over a period of 72 h significantly reduced the viability of all HPV^+ cell lines tested—20-30% reduction in HeLa; 30-40% in CaSki, and 75-85% in NOKE6/E7 ($P < 0.01$ and 0.001)—, whereas it was barely affected in HPV^- cells ($P > 0.05$) (Fig. 3a).

Next, we assessed the impact of SIRT1 inhibition on cell cycle by FACS analysis and found that—as expected in stressed cells expressing functional p53—the proportion of EX527-treated (48 h) HPV^+ cells arrested in the G_0/G_1 phase was increased by 5% to 13% ($P < 0.05$ and 0.01) compared to untreated cells, whereas no changes were observed in HPV^- cells (Fig. 3b).

To determine whether SIRT1 inhibition was also associated with a reduction in long-term proliferation, we performed colony-forming assays under identical conditions. As shown in Fig. 3c, the number of clones was reduced by 30% to 85% and their area by 50% to 80% in

EX527-treated HPV$^+$ cells compared to untreated cells ($P < 0.01$ and 0.001). By contrast, EX257 treatment did not affect long-term proliferation of both HPV$^-$ cell lines tested.

As the stress response may also activate a senescence program, a phenomenon very much dependent on the cellular context and stimuli, we also assessed senescence-associated β-gal (SA-β-gal) activity—a prototype marker of senescence—at neutral pH upon SIRT1 pharmacological inhibition, transient SIRT1 silencing, or transient E6/E7 silencing in HPV$^+$ cells. As shown in Fig. 3d and Supplementary Fig. S2, we failed to see any significant changes in the number of SA-β-gal-positive HeLa and CaSki cells upon SIRT1 pharmacological inhibition at different time points in comparison with vehicle-treated cells (Fig. 3d, upper and middle left panels). Upon transient silencing of SIRT1, an increase in SA-β-gal-positive cells was observed in HeLa cells at 72 h post-transfection but not in CaSki cells, albeit to much lower extent than that seen in the same cells silenced for E6/E7 expression (11% *vs* 54%, respectively) (Fig. 3d, upper and middle right panel). A slightly different picture emerged in NOKE6/E7 cells where the number of SA-β-gal-positive cells was already augmented upon SIRT1 inhibition, but again, at a lower extent when compared to E6/E7-silenced cells, especially at the 96-h time point (5% *vs* 15%) (Fig. 3d, lower panels). A similar trend was observed upon SIRT1 silencing in NOKE6/E7 cells in which a slight senescence induction was observed at 72 h post-transfection (Fig. 3d, lower right panel). As expected, transient silencing of E6 and E7 expression by RNA interference significantly increased the number of the SA-β-gal-positive cells in all three cell lines at both 72 and 96 h post-transfection (Fig. 3d, right panels) [51]. Altogether, the higher rate of senescence induction in E6/E7- *vs* SIRT1-silenced cells suggests that different mechanisms are involved.

To confirm the central role of p53 in the antiproliferative effect of EX527 treatment, we assessed the levels of $p21^{CDKN1A}$ expression in EX527-treated HPV$^+$ cells in which p53 expression was transiently knocked down by transfection of a p53-specific siRNA (sip53). As

expected, we failed to detect $p21^{CDKN1A}$ induction in p53-silenced cells upon 48 h of EX527 treatment, while its expression was significantly upregulated in siRNA control (siCtrl)-transfected cells (Fig. 3e and 3f). When we examined the expression levels of the viral oncoproteins E6 and E7 in sip53- *vs* siCtrl-transfected HPV^+ cell lines following EX527 treatment, E6 and, to a lesser extent, E7 were restored in HeLa cells, only E7 was partially restored in CaSki cells, while both proteins remained downregulated in NOKE6/E7 cells (Fig. 3e and 3f). In addition, cell cycle analysis confirmed that the number of cells arrested in G_0/G_1 upon EX527 treatment in siCtrl-transfected cells was significantly higher when compared to untreated cells (from 69 to 73% in HeLa, from 72 to 75% in CaSki, and from 68 to 74% in NOKE6/E7), while no major changes in cell cycle distribution upon EX527 treatment were observed in p53-silenced cells *vs* their untreated counterparts (from to 54 to 55% in HeLa, from 62 to 63% in CaSki, and from 52 to 57% in NOKE6/E7) (Fig. 3g). Consistent with the lack of growth inhibition, we observed an increased percentage of cells in S (from 8 to 14% in HeLa, from 10 to 15% in CaSki, and from 6 to 13% in NOKE6/E7) or G_2/M (from 6 to 15% in HeLa, from 7 to 10% in CaSki, and from 8 to 19% in NOKE6/E7) phase in EX527-treated sip53-transfected cells in comparison with siCtrl-transfected cells similarly treated.

These findings along with the observation that pharmacological inhibition of SIRT1 in p53-silenced HPV^+ cells did not lead to G_0/G_1 arrest, while E6 and E7 levels were poorly rescued, indicate that the antiproliferative action observed upon SIRT1 inhibition relies on p53 restoration. However, we cannot rule out that E6 and E7 depletion, for which we do not have a clear mechanistic explanation yet, may also play a role.

SIRT1 inhibition enhances the sensitivity of HPV^+ cells to genotoxic agents both *in vitro* and in a syngeneic mouse model of HPV16-induced cancer

Having discovered that SIRT1 inhibition restores a functional p53 in HPV^+ cells, we next asked whether this restoration had any impact on the sensitivity of these cells to genotoxic agents, *i.e.*, doxorubicin (DX) and cisplatin (Cis). To this end, cells were pretreated with EX527 or with vehicle alone for 24 h and then incubated with sublethal doses of DX or Cis. These doses were chosen based on a sublethal dose assessment (Supplementary Fig. S3). To rule out any bias related to the fact that the two cancer-derived cell lines used have been cultured for decades, we have also included the UPCI:SCC152 cell line (for brevity SCC152), which has been more recently generated from an HPV^+ HNSCC [52]. Assessment of cell viability over a period of 72 h post exposure revealed that EX527 pretreatment significantly enhanced drug-induced growth suppression of all three HPV^+ cell lines examined—8-42% and 10-32% growth reduction in EX527+DX- or EX527+Cis-treated cells, respectively, compared to cells treated with DX or Cis alone ($P < 0.05$, 0.01 and 0.001). Consistent with the data obtained with EX527 treatment alone (Fig. 3a), the highest reduction in cell viability occurred in the precancerous model of NOKE6/E7 cells (Fig. 4a). In contrast, no significant changes in growth inhibition were observed in the HPV^- cell lines C33A and HNO150 upon the combinatorial treatment compared to each single treatment. We also assessed the proportion of cells undergoing apoptosis upon single or combined treatment by flow cytometry analysis using annexin V/propidium iodide (PI) staining. As depicted in Fig. 4b, the percentage of apoptosis observed upon the combined treatment with EX527 and DX or Cis was respectively increased by 7% and 6% in HeLa, 10% and 5% in CaSki, 11% and 12% in NOKE6/E7, and 4% and 6% in SCC152 in comparison with each genotoxic treatment alone. Congruently, no changes were observed in the HPV^- cell lines when the combinatorial treatment was compared with the single treatment.

These sets of experiments consistently support the hypothesis that SIRT1 upregulation is a key mechanism of HPV-driven oncogenesis, and that the inhibition of such process by

EX527 treatment alone boosts cell cycle arrest and death of HPV^+ cell lines while increasing their sensitivity to the antiproliferative activity of standard chemotherapeutic agents [7, 53].

Thus, we next analyzed the therapeutic potential of combining EX527 and cisplatin *in vivo* using a syngeneic mouse model obtained by dorsal subcutaneous injection (s.c.) of C3.43 cells, which harbor an integrated HPV16 genome, in C57BL/6J mice. These cells were generated by transfecting mouse embryonic cells with a plasmid harboring the full-length HPV16 genome and extensively used for anti-HPV vaccine testing [34-36]. Upon s.c. injection of 1 x 10^6 cancer cells, palpable tumors were detectable after approximately one week when intra-peritoneal (i.p.) drug injection (mono or combination therapies) was started and repeated every second day up to 19 days after cancer cell injection (Fig. 5a). Keeping the same dose of EX527, we used decreasing doses of Cis (0.5, 1, or 2.5 mg/kg) to mimic the conditions of a de-escalating strategy. C3.43 cells robustly gave rise to tumor formation in vehicle-treated control mice, and tumor size effectively shrank upon i.p. administration of the drugs. Specifically, tumors arising in mice that had received the highest Cis dose grew significantly smaller already with monotherapy alone, while the lowest dose only exerted a modest growth inhibitory effect either alone or in combination with EX527. Notably, the tumors arising in mice injected with a combination of intermediate Cis dose (1 mg/kg) and EX527 (n=4) grew significantly smaller when compared to each of the monotherapy, either Cis or EX527 alone, as measured overtime by means of a Vernier caliper and evident at the visual inspection of the harvested tumors (Fig. 5b). The same trend was observed when the tumor weight of the explanted tumors was assessed at 19 days post-injection (Fig. 5c). Based on these results, we chose the intermediate dose of 1 mg/kg to statistically validate the efficacy of this combinatorial treatment in 4 additional mice, and the results obtained in n=8 mice confirmed the strong anticancer activity of Cis and EX527 combinatorial treatment as reported in Fig. 5d and 5f. To determine whether the responsiveness of C3.43 cells to the combinatorial treatment *in vivo* also involved p53 restoration, tissue

sections from the FFPE blocks of the explanted tumors were stained for p53 expression by immunohistochemistry. Similar to our *in vitro* results, a significantly increased number of p53-positive cells were found in the tumors harvested from mice injected with EX527 *vs* vehicle alone (Fig. 5g). Consistent with p53 restoration and the antiproliferative activity of EX527, quantification of the number of cells positive for the cellular proliferation marker Ki67 showed a significant reduction in the tumors from EX527- *vs* vehicle-treated mice.

Taken all together, these results indicate that combining Cis with EX527 treatment leads to effective reduction in tumor burden *in vivo* as well.

DISCUSSION

In the present study, we unveil an additional cellular pathway exploited by high-risk HPVs to effectively inhibit p53, with a central role played by the cellular deacetylase SIRT1 (Fig. 6). Furthermore, we present compelling *in vitro* and *in vivo* evidence demonstrating that targeting this pathway can sensitize HPV^+ tumor cells to standard genotoxic agents. These findings open up the possibility of using SIRT1 inhibitors as part of de-escalation therapies, aiming to reduce treatment-associated morbidity in patients with HPV-associated cancer, particularly those with OPSCC [7-10]. Indeed, HPV^+ OPSCC has one of the most rapidly increasing incidences among cancers in high-income countries and is characterized by improved prognosis and higher prevalence in younger patients. As a result, there is a growing interest in developing targeted therapies and de-intensification strategies to enhance the quality of life while maintaining acceptable survival outcomes [1-6].

While the role of SIRT1 in regulating p53 stability through deacetylation has been extensively studied (*i.e.*, p53 acetylation at K382 competes against ubiquitination, promoting p53 stabilization and activation), its involvement in E6/E7-driven oncogenesis is a novel finding [22, 23, 28, 29] (Fig. 2). Likewise, SIRT1 has already been shown to be upregulated in

474 HPV-infected cells being a crucial regulator of multiple aspects of the high- risk HPV life
475 cycle, while its role in p53 inactivation was unknown [24].

476 SIRT1, the primary NAD^+-dependent deacetylase in mammalian cells, exerts its
477 function by deacetylating various substrates, including histone substrates and non-histone
478 targets, such as p53, the acetylation of which on K382 lysine residue is critical for both protein
479 stabilization and transcriptional activity [17-23]. In line with its role in promoting p53
480 degradation in HPV^+ cell lines, we show that SIRT1 inactivation, either by the specific
481 pharmacological inhibitor EX527 (also known as Selisistat) or gene silencing, leads to
482 increased p53 protein expression levels. SIRT1 specifically deacetylates the K382 residue of
483 p53 and, accordingly, its inactivation leads to increased Ac-p53 (K382) expression levels in
484 both HPV^+ and HPV^- cell lines [28, 29]. However, when we assessed the impact of restored
485 p53 on the growth of HPV^+ *vs* HPV^- cell lines upon pharmacological inhibition of SIRT1, we
486 observed impaired cell viability and proliferation rates only in HPV^+ cells, confirming the
487 functional role of p53 in HPV^+ but not HPV^- cancer cells (Fig. 3a). Accordingly, restored p53
488 in HPV^+ cell lines exhibited transcriptional activity as evidenced by the upregulation of the
489 down-stream effector protein $p21^{CDKN1A}$ and the enrichment of both p53 and Ac-p53 (K382)
490 at its promoter region. Importantly, the $p21^{CDKN1A}$ promoter region also displayed
491 accumulation of H3K9Ac, consistent with its transcriptionally active state (Fig. 2g). Indeed,
492 binding of Ac-p53 (K382) to the $p21^{CDKN1A}$ promoter region has been shown to recruit histone-
493 acetyltransferases, which contributes to euchromatin formation by targeting histones [31]. In
494 good agreement with the rescue of the p53/ $p21^{CDKN1A}$ axis in HPV^+ cell lines, we found them
495 to be arrested at the G_0/G_1 phase in response to SIRT1 inhibition (Fig. 3b) [30]. Even though
496 SIRT1 pharmacological inhibition steadily downregulated the expression levels of the viral
497 oncoproteins E6 and E7, we failed to see any enhancement of SA-β-gal activity, a hallmark of
498 senescence, in both HeLa and CaSki cells, while a robust senescence induction was observed

upon transient gene silencing of E6 and E7 (Fig. 3d and Supplementary Fig. S2) [15, 51]. In the case of NOKE6/E7, some degree of senescence was seen upon EX527 treatment, albeit to a much lower extent than that observed upon E6/E7 silencing.

Taken together, these findings indicate that SIRT1 inhibition leads to growth arrest through a p53/ $p21^{CDKN1A}$-dependent mechanism, whereas E6/E7 silencing strongly induces senescence, likely via a different signaling pathway.

This scenario is further complicated by the fact that the molecular mechanisms responsible for inducing senescence upon E6/E7 depletion remain unknown, and the extent of inhibition of the viral oncoproteins may vary based on the chosen silencing or inactivation strategy. In addition, the mutation burden of the cancer cells, which is higher in human carcinoma-derived cell lines such as HeLa and CaSki cells and lower in immortalized cell lines like NOKE6/E7, may also influence the response of cancer cells to E6/E7 depletion. This distinction is also evident from the cell viability assays reported in this study, where the pharmacological inhibition of SIRT1 in HeLa and CaSki cells primarily manifests as cytostatic, while in NOKE6/E7 cells there is a progressive inhibition in cell viability coupled with the induction of apoptosis.

Along these lines, we show that EX527 treatment of p53-depleted cells does not restore $p21^{CDKN1A}$ expression levels or G_0/G_1 cell cycle arrest. Notably, under these conditions, only partial restoration of E6 and E7 oncoprotein expression is observed.

Another important finding from this study is the heightened sensitivity of NOKE6/E7 cells to SIRT1 inhibition compared to the cervical carcinoma-derived HeLa and CaSki cell lines. This is evident from the significant restoration of Ac-p53 (K382) expression levels, substantial downregulation of the viral oncoproteins E6 and E7, enhanced cell growth inhibition, and induction of apoptosis (Figs. 2 and 3). An explanation for this enhanced sensitivity could be that NOKE6/E7 cells represent early stages of HPV16-induced

524 oncogenesis, where the reliance on p53 suppression is known to be more pronounced [13, 14,
525 37].

526 The restoration of functional p53 tumor suppressor activity presents a significant
527 therapeutic opportunity in the treatment of HPV-driven cancer, given the unique characteristic
528 of this cancer model where p53 is seldom impaired by dysfunctional mutations. *TP53* is the
529 most frequently mutated gene in HPV^- OPSCC, occurring in at least 75% of patients. However,
530 *TP53* mutations are rarely observed in the context of HPV^+ disease, largely due to the inhibitory
531 effect of E6 on p53 function, allowing the virus to phenocopy this genetic alteration [2-7].
532 Consequently, HPV-associated cancers retain wild-type p53, which is inactivated by the
533 oncoprotein E6 forming a complex with the cellular ubiquitin ligase E6AP, which in turn
534 targets p53 for ubiquitination and proteasomal degradation [16, 33].

535 Building upon our earlier findings and the ability to counteract E6AP actions and
536 restore functional p53 through SIRT1 inhibition, we show that this treatment can strongly boost
537 the anticancer activity of genotoxic agents commonly used to treat HPV-associated cancers,
538 such as DX and Cis, which are frequently employed in the treatment of HPV-associated cancers
539 [7, 53]. Our results reveal that pharmacological inhibition of SIRT1 markedly increases cell
540 death when sublethal doses of these drugs are administered (Fig. 4). Remarkably, similar
541 observations were replicated in a syngeneic mouse model of HPV16-induced cancer. Tumor
542 samples obtained from mice treated systemically with EX527 exhibited significantly elevated
543 levels of p53 expression and decreased expression of the proliferation marker Ki67, as assessed
544 by immunohistochemistry, when compared to mice treated with the control vehicle (Fig. 5).

545 Similarly, Dell'Omo et al. connected the chemopreventive action of exisulind and
546 certain nonsteroidal anti-inflammatory drugs (NSAIDs), known for their anticancer properties,
547 to the direct inhibition of SIRT1 and the consequent activation of the p53/p21 anti-oncogenic
548 pathway. Using a mouse model of early mammary gland transformation, they demonstrated

549 that SIRT1 inhibition correlates with the *in vivo* ability of the aforementioned compounds to
550 activate p53 and hinder tissue proliferation in the initial stages of transformation [54].

551 In conclusion, our findings shed light on a previously unrecognized role of SIRT1
552 during HPV-driven oncogenesis and provide compelling evidence that inhibiting SIRT1 can
553 be used in combination with standard chemotherapies to enhance their anticancer efficacy.

554 Although our study does not specifically address the impact of SIRT1 inhibition in
555 combination with radiotherapy, it is well established that cells with functional p53 are more
556 susceptible to radiation-induced cell death [55]. Therefore, it is highly likely that SIRT1
557 inhibition can enhance the anticancer activity of radiotherapy as well.

558 Given that current treatment options for cervical cancer and HNC (*i.e.*, radiotherapy,
559 chemotherapy, and surgery) have significant detrimental effects on the targeted anatomical
560 sites, exploring alternative therapies with fewer side effects is crucial for improving patient
561 outcomes [7, 53]. The proposed combinatorial treatment for HPV^+ cancer has the potential to
562 facilitate de-escalation strategies aimed at reducing the adverse effects of current radio-
563 chemotherapy-based therapies while improving treatment outcomes. Further preclinical
564 investigations are currently underway to translate this approach into clinical practice.

565

566 # ADDITIONAL INFORMATION

567 ## ACKNOWLEDGMENTS

568 We thank Marcello Arsura for critically reviewing the manuscript. NOKE6/E7 cells were
569 kindly provided by Martina Niebler and Frank Rösl, German Cancer Research Center (DKFZ)-
570 Heidelberg and C3.43 cells by Martin Kast, University of Southern California in Los Angeles.
571 We are also grateful to Michela Salvo from the Histology Research Core Facility at University
572 of Piemonte Orientale (Novara, Italy) for technical support in tissue processing and histological
573 analysis, Nausicaa Clemente from the Department of Health Sciences at University of

Piemonte Orientale (Novara, Italy) for technical support to perform *in vivo* experiments, and Valeria Caneparo at CAAD, Center for Translational Research and Autoimmune and Allergic Disease, for assistance in SA-β-gal analysis.

AUTHORS' CONTRIBUTIONS

I. Lo Cigno: Conceptualization, data curation, investigation, methodology, project administration, software, validation, writing–original draft. **F. Calati:** Conceptualization, data curation, investigation, methodology, writing–original draft. **C. Girone:** Data curation, investigation, methodology. **C. Borgogna:** Formal analysis, project administration, supervision, writing–review and editing. **A. Venuti:** Resources, validation, writing–review and editing. **R. Boldorini:** Investigation, validation, writing–review and editing. **M. Gariglio:** Conceptualization, supervision, funding acquisition, writing–original draft, writing–review and editing.

ETHICS APPROVAL

The mice used for the *in vivo* tumorigenicity assays were housed in our animal facilities in accordance with "The Guide for the Care and Use of Laboratory Animals", and the experimentation was approved by the Italian Ministry of Health (Agreement No. 219/2020-PR).

CONSENT FOR PUBLICATION

This manuscript has not been previously published and is not under consideration for publication elsewhere.

DATA AVAILABILITY

All data generated or analyzed during this study are included either in this article or in additional files, and the links to public datasets are reported in the manuscript.

COMPETING INTERESTS

I. Lo Cigno, F. Calati, and M. Gariglio report the Italian Patent No. 102020000023281 issued in October 2nd, 2020 ("SIRT1 INHIBITOR OR ANTAGONIST FOR USE IN PREVENTING AND/OR TREATING AN HPV-INDUCED TUMOUR"). This patent is pending for the international patent application approval (PCT/IB2021/059055). All the other authors declare no competing financial interests.

FUNDING INFORMATION

This work was supported by the Italian Ministry for University and Research-MIUR (20178ALPCM-PRIN 2017 to MG), the AGING Project–Department of Excellence–DIMET, University of Piemonte Orientale, Associazione Italiana per la Ricerca sul Cancro-AIRC (25767-IG 2021 to MG), and Next Generation EU - PNRR M6C2 - Investimento 2.1 Valorizzazione e potenziamento della ricerca biomedica del SSN (PNRR-MAD-2022-12376570 to MG). The funders had no role in study design, data collection and analysis, decision to publish, or preparation of the manuscript.

REFERENCES

1. Berman TA, Schiller JT. Human papillomavirus in cervical cancer and oropharyngeal cancer: One cause, two diseases. *Cancer* **123**, 2219-29 (2017).
2. Lechner M, Liu J, Masterson L, Fenton TR. HPV-associated oropharyngeal cancer: epidemiology, molecular biology and clinical management. *Nat Rev Clin Oncol* **19**, 306-27 (2022).

3. Shewale JB, Gillison ML. Dynamic factors affecting HPV-attributable fraction for head and neck cancers. *Curr Opin Virol* **39**, 33-40 (2019).
4. Johnson DE, Burtness B, Leemans CR, Lui VWY, Bauman JE, Grandis JR. Head and neck squamous cell carcinoma. *Nat Rev Dis Primers* **6(1)**, 92 (2020).
5. Guo T, Kang SY, Cohen EEW. Current perspectives on recurrent HPV-mediated oropharyngeal cancer. *Front Oncol* **12**, 966899 (2022).
6. Chow LQM. Head and Neck Cancer. *N Engl J Med* **382**, 60-72 (2020).
7. Caudell JJ, Gillison ML, Maghami E, Spencer S, Pfister DG, Adkins D, et al. NCCN Guidelines® Insights: Head and Neck Cancers, Version 1.2022. *J Natl Compr Canc Netw* **20**, 224-34 (2022).
8. Harari PM. Open the Gates for Treatment De-Intensification in Head and Neck Cancer. *J Clin Oncol* **37**, 1854-55 (2019).
9. Bates JE, Steuer CE. HPV as a Carcinomic Driver in Head and Neck Cancer: a De-escalated Future? *Curr Treat Options Oncol* **23**, 325-32 (2022).
10. Orlandi E, Licitra L. Personalized Medicine and the Contradictions and Limits of First-Generation Deescalation Trials in Patients With Human Papillomavirus-Positive Oropharyngeal Cancer. *JAMA Otolaryngol Head Neck Surg* **144**, 99-100 (2018).
11. McBride AA. Human papillomaviruses: diversity, infection and host interactions. *Nat Rev Microbiol* **20**, 95-108 (2022).
12. Doorbar J, Quint W, Banks L, Bravo IG, Stoler M, Broker TR, et al. The biology and life-cycle of human papillomaviruses. *Vaccine* **30**, F55-70 (2012).
13. Moody CA, Laimins LA. Human papillomavirus oncoproteins: pathways to transformation. *Nat Rev Cancer* **10**, 550-60 (2010).
14. Mittal S, Banks L. Molecular mechanisms underlying human papillomavirus E6 and E7 oncoprotein-induced cell transformation. *Mutat Res Rev Mutat Res* **772**, 23-35 (2017).

15. Hoppe-Seyler K, Bossler F, Braun JA, Herrmann AL, Hoppe-Seyler F. The HPV E6/E7 Oncogenes: Key Factors for Viral Carcinogenesis and Therapeutic Targets. *Trends Microbiol* **26**, 158-68 (2018).
16. Hebner C, Beglin M, Laimins LA. Human papillomavirus E6 proteins mediate resistance to interferon-induced growth arrest through inhibition of p53 acetylation. *J Virol* **81**, 12740-7 (2007).
17. Liu TF, McCall CE. Deacetylation by SIRT1 Reprograms Inflammation and Cancer. *Genes Cancer* **4**, 135-47 (2013).
18. Lin Z, Fang D. The Roles of SIRT1 in Cancer. *Genes Cancer* **4**, s97-104 (2013).
19. Kwon HS, Ott M. The ups and downs of SIRT1. *Trends Biochem Sci* **33**, 517-25 (2008).
20. Gomes AR, Yong JS, Kiew KC, Aydin E, Khongkow M, Laohasinnarong S, et al. Sirtuin1 (SIRT1) in the Acetylation of Downstream Target Proteins. *Methods Mol Biol* **1436**, 169-88 (2016).
21. Zhang T, Kraus WL. SIRT1-dependent regulation of chromatin and transcription: linking NAD(+) metabolism and signaling to the control of cellular functions. *Biochim Biophys Acta* **1804**, 1666-75 (2010).
22. Vaziri H, Dessain SK, Ng Eaton E, Imai SI, Frye RA, Pandita TK, et al. hSIR2(SIRT1) functions as an NAD-dependent p53 deacetylase. *Cell* **107**, 149-59 (2001).
23. Lee JT, Gu W. SIRT1: Regulator of p53 Deacetylation. *Genes Cancer* **4**, 112-7 (2013).
24. Langsfeld ES, Bodily JM, Laimins LA. The Deacetylase Sirtuin 1 Regulates Human Papillomavirus Replication by Modulating Histone Acetylation and Recruitment of DNA Damage Factors NBS1 and Rad51 to Viral Genomes. *PLoS Pathog* **11**, e1005181 (2015).
25. Das D, Smith N, Wang X, Morgan IM. The Deacetylase SIRT1 Regulates the Replication Properties of Human Papillomavirus 16 E1 and E2. *J Virol* **91**, e00102-17 (2017).

673 26. Velez-Perez A, Wang XI, Li M, Zhang S. SIRT1 overexpression in cervical squamous
674 intraepithelial lesions and invasive squamous cell carcinoma. *Hum Pathol* **59**, 102-7
675 (2017).
676 27. So D, Shin HW, Kim J, Lee M, Myeong J, Chun YS, et al. Cervical cancer is addicted to
677 SIRT1 disarming the AIM2 antiviral defense. *Oncogene* **37**, 5191-204 (2018).
678 28. Solomon JM, Pasupuleti R, Xu L, McDonagh T, Curtis R, DiStefano PS, et al. Inhibition
679 of SIRT1 catalytic activity increases p53 acetylation but does not alter cell survival
680 following DNA damage. *Mol Cell Biol* **26**, 28-38 (2006).
681 29. Yi J, Luo J. SIRT1 and p53, effect on cancer, senescence and beyond. *Biochim Biophys*
682 *Acta* **1804**, 1684-9 (2010).
683 30. Atkins KM, Thomas LL, Barroso-González J, Thomas L, Auclair S, Yin J, et al. The
684 multifunctional sorting protein PACS-2 regulates SIRT1-mediated deacetylation of p53 to
685 modulate p21-dependent cell-cycle arrest. *Cell Rep* **8**, 1545-57 (2014).
686 31. Barlev NA, Liu L, Chehab NH, Mansfield K, Harris KG, Halazonetis TD, et al. Acetylation
687 of p53 activates transcription through recruitment of coactivators/histone
688 acetyltransferases. *Mol Cell* **8**, 1243-54 (2001).
689 32. Tang Y, Zhao W, Chen Y, Zhao Y, Gu W. Acetylation is indispensable for p53 activation.
690 *Cell* **133**, 612-26 (2008).
691 33. Talis AL, Huibregtse JM, Howley PM. The role of E6AP in the regulation of p53 protein
692 levels in human papillomavirus (HPV)-positive and HPV-negative cells. *J Biol Chem* **273**,
693 6439-45 (1998).
694 34. Feltkamp MCW., Smits HL, Vierboom MPM, Minnaar RP, de Jongh BM, Drijfhout JW,
695 et al. Vaccination with cytotoxic T lymphocyte epitope-containing peptide protects against
696 a tumor induced by human papillomavirus type 16-transformed cells. *J. Immunol* **23**, 2242-
697 49 (1993).

698 35. Smith KA, Meisenburg BL, Tam VL, Pagarian RR, Wong R, Joea DK, et al. Lymph node
699 targeted immunotherapy mediates potent immunity resulting in regression of isolated or
700 disseminated HPV transformed tumors. *Clin Cancer Res* **15**, 6167-76 (2009).
701 36. Accardi L, Paolini F, Mandarino A, Percario Z, Di Bonito P, Di Carlo V, et al. In vivo
702 antitumor effect of an intracellular single-chain antibody fragment against the E7
703 oncoprotein of human papillomavirus 16. *Int J Cancer* **134**, 2742-7 (2014).
704 37. Yang R, Klimentová J, Göckel-Krzikalla E, Ly R, Gmelin N, Hotz-Wagenblatt A, et al.
705 Combined Transcriptome and Proteome Analysis of Immortalized Human Keratinocytes
706 Expressing Human Papillomavirus 16 (HPV16) Oncogenes Reveals Novel Key Factors
707 and Networks in HPV Induced Carcinogenesis. *mSphere* **4**, e00129-19 (2019).
708 38. Lo Cigno I, Calati F, Borgogna C, Zevini A, Albertini S, Martuscelli L, et al. Human
709 Papillomavirus E7 Oncoprotein Subverts Host Innate Immunity via SUV39H1-Mediated
710 Epigenetic Silencing of Immune Sensor Genes. *J Virol* **94**, e01812-9 (2020).
711 39. Lo Cigno I, De Andrea M, Borgogna C, Albertini S, Landini MM, Peretti A, et al. The
712 Nuclear DNA Sensor IFI16 Acts as a Restriction Factor for Human Papillomavirus
713 Replication through Epigenetic Modifications of the Viral Promoters. *J Virol* **89**, 7506-20
714 (2015).
715 40. Pauwels R, Balzarini J, Baba M, Snoeck R, Schols D, Herdewijn P, et al. Rapid and
716 automated tetrazolium-based colorimetric assay for the detection of anti-HIV compounds.
717 *J Virol Methods* **20**, 309-21 (1988).
718 41. Itahana K, Itahana Y, Dimri GP. Colorimetric detection of senescence-associated β
719 galactosidase. *Methods Mol Biol* **965**, 143–56 (2013).
720 42. Cancer Genome Atlas Network. Comprehensive genomic characterization of head and
721 neck squamous cell carcinomas. *Nature* **517**, 576-82 (2015).

722 43. Gertz M, Fischer F, Nguyen GT, Lakshminarasimhan M, Schutkowski M, Weyand M, et
723 al. Ex-527 inhibits Sirtuins by exploiting their unique NAD+-dependent deacetylation
724 mechanism. *Proc Natl Acad Sci U S A* **110**, E2772-81 (2013).
725 44. Meissner JD. Nucleotide sequences and further characterization of human papillomavirus
726 DNA present in the CaSki, SiHa and HeLa cervical carcinoma cell lines. *J Gen Virol* **80**,
727 1725-33 (1999).
728 45. Abdulkarim B, Sabri S, Deutsch E, Chagraoui H, Maggiorella L, Thierry J, et al. Antiviral
729 agent Cidofovir restores p53 function and enhances the radiosensitivity in HPV-associated
730 cancers. *Oncogene* **21**, 2334-46 (2002).
731 46. Ninck S, Reisser C, Dyckhoff G, Helmke B, Bauer H, Herold-Mende C. Expression
732 profiles of angiogenic growth factors in squamous cell carcinomas of the head and neck.
733 *Int J Cancer* **106**, 34–44 (2003).
734 47. Scheffner M, Münger K, Byrne JC, Howley PM. The state of the p53 and retinoblastoma
735 genes in human cervical carcinoma cell lines. *Proc Natl Acad Sci U S A* **88**, 5523-7 (1991).
736 48. Srivastava S, Tong YA, Devadas K, Zou ZQ, Chen Y, Pirollo KF, et al. The status of the
737 p53 gene in human papilloma virus positive or negative cervical carcinoma cell lines.
738 *Carcinogenesis* **13**, 1273-5 (1992).
739 49. Piboonniyom SO, Duensing S, Swilling NW, Hasskarl J, Hinds PW, Münger K. Abrogation
740 of the retinoblastoma tumor suppressor checkpoint during keratinocyte immortalization is
741 not sufficient for induction of centrosome-mediated genomic instability. *Cancer Res* **63**,
742 476-83 (2003).
743 50. Vaquero A, Scher M, Lee D, Erdjument-Bromage H, Tempst P, Reinberg D. Human SirT1
744 interacts with histone H1 and promotes formation of facultative heterochromatin. *Mol Cell*
745 **16**, 93-105 (2004).

51. Hall AH, Alexander KA. RNA interference of human papillomavirus type 18 E6 and E7 induces senescence in HeLa cells. *J Virol* **77**, 6066-9 (2003).
52. Olthof NC, Huebbers CU, Kolligs J, Henfling M, Ramaekers FC, Cornet I, et al. Viral load, gene expression and mapping of viral integration sites in HPV16-associated HNSCC cell lines. *Int J Cancer* **136(5)**, E207-18 (2015).
53. Rose PG. Concurrent cisplatin-based radiotherapy and chemotherapy for locally advanced cervical cancer. *N Engl J Med* **341**, 708 (1999).
54. Dell'Omo G, Crescenti D, Vantaggiato C, Parravicini C, Borroni AP, Rizzi N, et al. Inhibition of SIRT1 deacetylase and p53 activation uncouples the anti-inflammatory and chemopreventive actions of NSAIDs. *Br J Cancer* **120**, 537-546 (2019).
55. Kong X, Yu D, Wang Z, Li S. Relationship between p53 status and the bioeffect of ionizing radiation. *Oncol Lett* **22**, 661 (2021).

FIGURE LEGENDS

Fig. 1 SIRT1 gene expression and status in HPV$^+$ *vs* HPV$^-$ head and neck squamous cell carcinoma (HNSCC).

a TCGA-curated clinical data set of HNSCC (279 patients and samples) was interrogated for samples harboring genomic SIRT1 or *TP53* mutations. HPV status scores corresponding to each clinical specimen are shown [42]. **b** Boxplot illustrating the comparison of SIRT1 mRNA expression levels between HPV$^+$ and HPV$^-$ HNSCCs in the TCGA dataset. ***$P < 0.001$, unpaired t-test [42].

Fig. 2 Pharmacological and genetic inhibition of SIRT1 activity restores Ac-p53 (K382) protein expression.

a Cells were treated with EX527 (80 μM) or vehicle (DMSO). At the indicated time points after treatment, total cell extracts were subjected to immunoblot analysis with anti-SIRT1, anti-p53, anti-acetylated p53 (Lys382 or Lys305), anti-p21^{CDKN1A}, anti-p16^{INK4a}, anti-HPV16 or HPV18 E6, anti-HPV16 or HPV18 E7, and anti-GAPDH antibodies as loading control. **b** The intensities of the bands for the indicated antibody were quantified by densitometry, and ratios of the abundance of these proteins relative to that of GAPDH were calculated. Values are representative of three independent experiments. Error bars indicate SD. *$P < 0.05$, **$P < 0.01$, unpaired t-test. **c** Quantitation of Ac-p53 (K382) levels relative to total p53 is shown. Values are representative of three independent experiments. Error bars indicate SD. *$P < 0.05$, unpaired t-test. **d** Immunoblot analysis of total cell extracts from HeLa, CaSki, and NOKE6/E7 cells transfected with siSIRT1 or siCtrl for 72 h was performed by using the same panel of antibodies listed in panel A. **e** Densitometric analysis showing fold change expression of the indicated proteins from three independent experiments. Error bars indicate SD. *$P < 0.05$, **$P < 0.01$, unpaired t-test. **f** Quantitation of Ac-p53 (K382) levels relative to total p53 is shown. Values are representative of three independent experiments. Error bars indicate SD. **g** Extracts

were prepared from HeLa, CaSki, and NOKE6/E7 cells treated for 48 h with EX527 (80 μM) or vehicle (DMSO). ChIP assay was carried out using antibodies specific for unmodified histone H3 (PAN-H3), acetylated lysine 9 of H3 (H3K9Ac), p53, and acetylated lysine 382 of p53 [Ac-p53 (K382)], or IgG as control. Immunoprecipitated promoter sequences were measured by qPCR, and CT values for the samples were equated to input CT values. Values are represented as input percentage from three independent experiments. Error bars indicate SD *$P < 0.05$, **$P < 0.01$, unpaired t-test.

Fig. 3 Restoration of a functional Ac-p53 (K382) inhibits the growth of HPV$^+$ cells.

a Cells were treated with EX527 (80 μM) or with vehicle (DMSO) and then cell viability was determined by MTT assay at the indicated time points. The data shown are representative of three independent experiments. Error bars indicate SD. ** $P < 0.01$, *** $P < 0.001$, unpaired t-test. **b** Cell cycle distribution of cells treated with EX527 (80 μM) or with vehicle (DMSO) for 48 h was assessed by flow cytometry. G_0/G_1 phase of the cell cycle is graphically shown for each cell line. Data shown are representative of three independent experiments. Error bars indicate SD. * $P < 0.05$, ** $P < 0.01$, unpaired t-test. **c** Representative images of anchorage-dependent colony formation assay (CFA) of HeLa, CaSki, NOKE6/E7, C33A, and HNO150 cells treated with EX527 (80 μM), or vehicle (DMSO) for 15 days. The percentages of colony number and area are indicated in the right panels as mean values of three biological triplicates. Error bars indicate SD. **$P < 0.01$, *** $P < 0.001$, unpaired t-test. **d** Senescence-associated beta-galactosidase activity (SA-β-gal) was assessed in HeLa, CaSki, and NOKE6/E7 cells treated with EX527 (80 μM) or vehicle (DMSO), or transfected with siCtrl, siE6E7, or siSIRT1 for the indicated time points. The percentage of SA-β-gal-positive cells is shown as mean values of three biological triplicates. Error bars indicate SD. * $P < 0.05$, **$P <$ 0.01, *** $P < 0.001$, unpaired t-test. **e** Total cell extracts from HeLa, CaSki, and NOKE6/E7 cells transfected for 24 h with sip53 or siCtrl and subsequently treated with EX527 (80 μM),

or vehicle (DMSO) for 48 h were subjected to immunoblot analysis for the indicated proteins. **f** The intensities of the bands for each antibody were quantified by densitometry, and abundance ratios of these proteins relative to that of GAPDH were calculated. Values are representative of three independent experiments. Error bars indicate SD. *$P < 0.05$, ** $P < 0.01$, unpaired t-test. **G,** Cell cycle distribution of the cells described in panel F was assessed by flow cytometry. The results are representative of three independent experiments. Error bars indicate SD. * $P < 0.05$, ** $P < 0.01$, unpaired t-test.

Fig. 4 SIRT1 inhibition enhances the sensitivity of HPV$^+$ cells to genotoxic agents.

a Cells were treated with EX527 (80 μM) or with vehicle (DMSO) for 24 h and then mock-treated or treated with doxorubicin (1.5 μM for HeLa, NOKE6/E7, SCC152, C33A, and HNO150, and 0.5 μM for CaSki) or cisplatin (10 μM for HeLa, 15 μM for CaSki, C33A, and HNO150, 2.5 μM for NOKE6/E7, and 5 μM for SCC152) for the indicated time points. Cell proliferation was determined by MTT assay in three biological replicates. Error bars indicate SD. *$P < 0.05$, **$P < 0.01$, *** $P < 0.001$, unpaired *t* test. **b** Cells described in panel A were incubated with Annexin V-FITC in a buffer containing propidium iodide (PI) and analyzed by flow cytometry. Graphs show the percentage of cells in early apoptosis (annexin V–positive and PI-negative) and late apoptosis/necrosis (annexin V–positive and PI–positive). Data shown are presented as mean values of biological triplicates. Error bars indicate SD *$P < 0.05$, **$P < 0.01$, *** $P < 0.001$, unpaired t-test.

Fig. 5 EX527 enhances cisplatin cytotoxic activity in an *in vivo* syngeneic mouse model of HPV16-induced cancer.

a Schematic illustration of the tumor model in which C3.43 cells were subcutaneously inoculated into the back of C57BL/6J mice. EX527 (10 mg/kg) and/or cisplatin (0.5, 1, 2.5 mg/kg) were administered intraperitoneally from day 7 after cancer cell injection, with one dose every two days up to day 19, when the tumors were harvested. **b** Tumor volumes from

mice (n=4 each group) treated as indicated in panel A were measured every two days and reported as mean volume of 4 tumors for each treatment. Statistical analysis was carried out by comparing each treatment vs vehicle. SD. *$P < 0.05$ (for vehicle *vs* Cis 1 mg/kg and vehicle *vs* EX527+Cis 1 mg/kg), **$P < 0.01$ (for vehicle *vs* Cis 2.5 mg/kg and vehicle *vs* EX527+Cis 2.5 mg/kg), unpaired t-test. **c** Tumor weights from mice treated as indicated in panel A were determined at the endpoint of the experiment. Each dot represents data from a mouse. Error bars indicate SD. *$P < 0.05$, **$P < 0.01$, unpaired t-test. **d** Tumor volumes from mice (n=8 each group) injected i.p. with EX527 (10 mg/kg) and cisplatin (1 mg/kg), either combined or single treatment, were measured every two days and reported as mean volume of 8 tumors for each treatment. Error bars indicate SD. *$P < 0.05$, *** $P < 0.001$, unpaired t-test. **e** Tumor weights from mice treated as described in panel D were determined at the endpoint of the experiment. Each dot represents data from a mouse. Error bars indicate SD. ***$P < 0.001$, unpaired t-test. **f** Representative images of tumors for each treatment from mice treated as indicated in panel D. **g** Representative H&E and IHC staining for p53 and Ki67 antibody performed on tumors treated with vehicle or EX527 (Scale bars: 20 μm). Quantitative cell image analysis was carried out on tissue samples viewed at 40x magnification. Automatic quantitation of positive nuclei count of stained sections was performed using QuPath v0.2.6. For each slide, cells with nuclear staining were counted in six random non-adjacent areas, and results from the 6 areas were averaged to generate a percentage of positive cells per mm^2. The percentages of positive cells/mm^2 of each slide were then averaged and plotted. Error bars indicate SD. *** $P < 0.001$, unpaired t-test.

Fig. 6 Schematic model depicting the molecular circuitry governing p53 functions via SIRT1-mediated acetylation in HPV$^+$ cells. The left part of the diagram illustrates the molecular interplay involving the p53 protein ubiquitinated at position K382, the viral oncoprotein E6, and the cellular ubiquitin ligase E6AP, which leads to p53 degradation under

normal conditions in HPV$^+$ cells. The right part of the diagram depicts the impact of SIRT1 inhibition on p53 acetylation. With SIRT1 inhibited either pharmacologically (e.g., using the specific inhibitor EX527) or through genetic silencing (e.g., siRNA), the acetylation of lysine at position K382 persists, rendering it inaccessible for ubiquitination, leading to p53 restoration.

Figure S1. Restoration of the p53/p21 pathway observed upon EX527 treatment is not associated with circadian effects. NOKE6/E7 cells were treated with EX527 (80 μM) or vehicle (DMSO) for the indicated time points, and then total cell extracts were subjected to immunoblot analysis with anti-p53, anti-p21^{CDKN1A}, or anti-GAPDH antibodies as loading control. One representative Western blot from three independent triplicates is shown.

Figure S2. Differential induction of senescence-associated beta-galactosidase activity (SA-β-gal) in HPV$^+$ cells upon SIRT1 inhibition or E6/E7 depletion. Representative images of HeLa, CaSki, and NOKE6/E7 cells treated with EX527 (80 μM) or vehicle (DMSO), or transfected with siCtrl, siE6E7, or siSIRT1 for the indicated time points.

Figure S3. Doxorubicin and cisplatin sublethal doses assessment. HeLa, CaSki, NOKE6/E7, SCC152, C33A, HNO150 cells were mock-treated or treated with various concentration of doxorubicin (0.5, 1.5, or 3 μM) **(a)** or cisplatin (2.5, 5, 10, 15 μM) **(b)** for 24 h. Cell proliferation was determined by MTT assay in three biological replicates. Error bars indicate SD. *$P < 0.05$, **$P < 0.01$, *** $P < 0.001$, unpaired t-test.

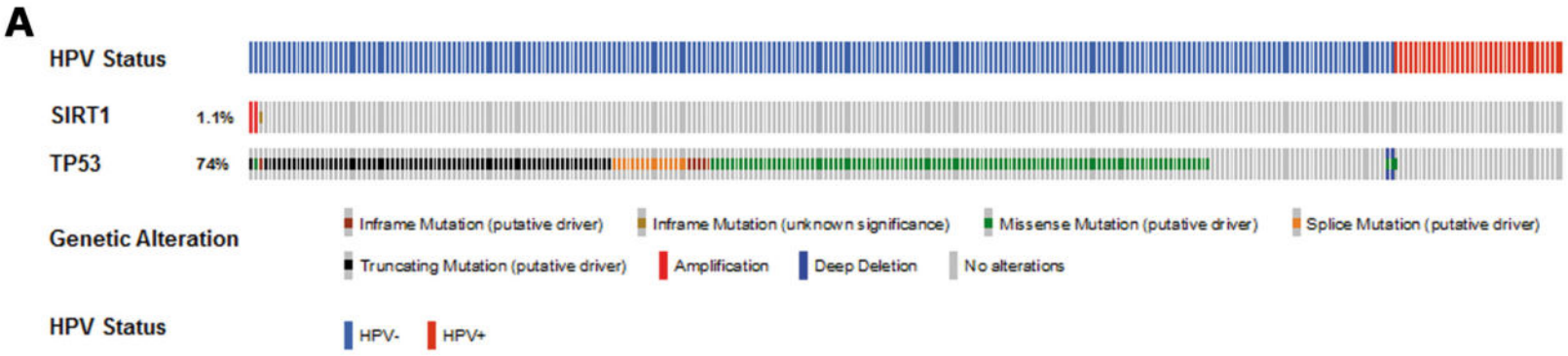
A
HPV Status
SIRT1
1.1%
TP53
74%
Genetic Alteration
Inframe Mutation (putative driver)
Inframe Mutation (unknown significance)
Missense Mutation (putative driver)
Splice Mutation (putative driver)
Truncating Mutation (putative driver)
Amplification
Deep Deletion
No alterations
HPV Status
HPV-
HPV+

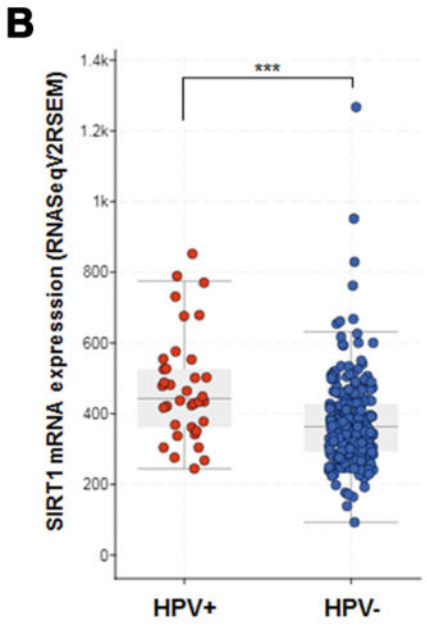
B
SIRT1 mRNA expresssion (RNASeqV2RSEM)
***
1.4k
1.2k
1k
800
600
400
200
0
HPV+
HPV-

Figure 1

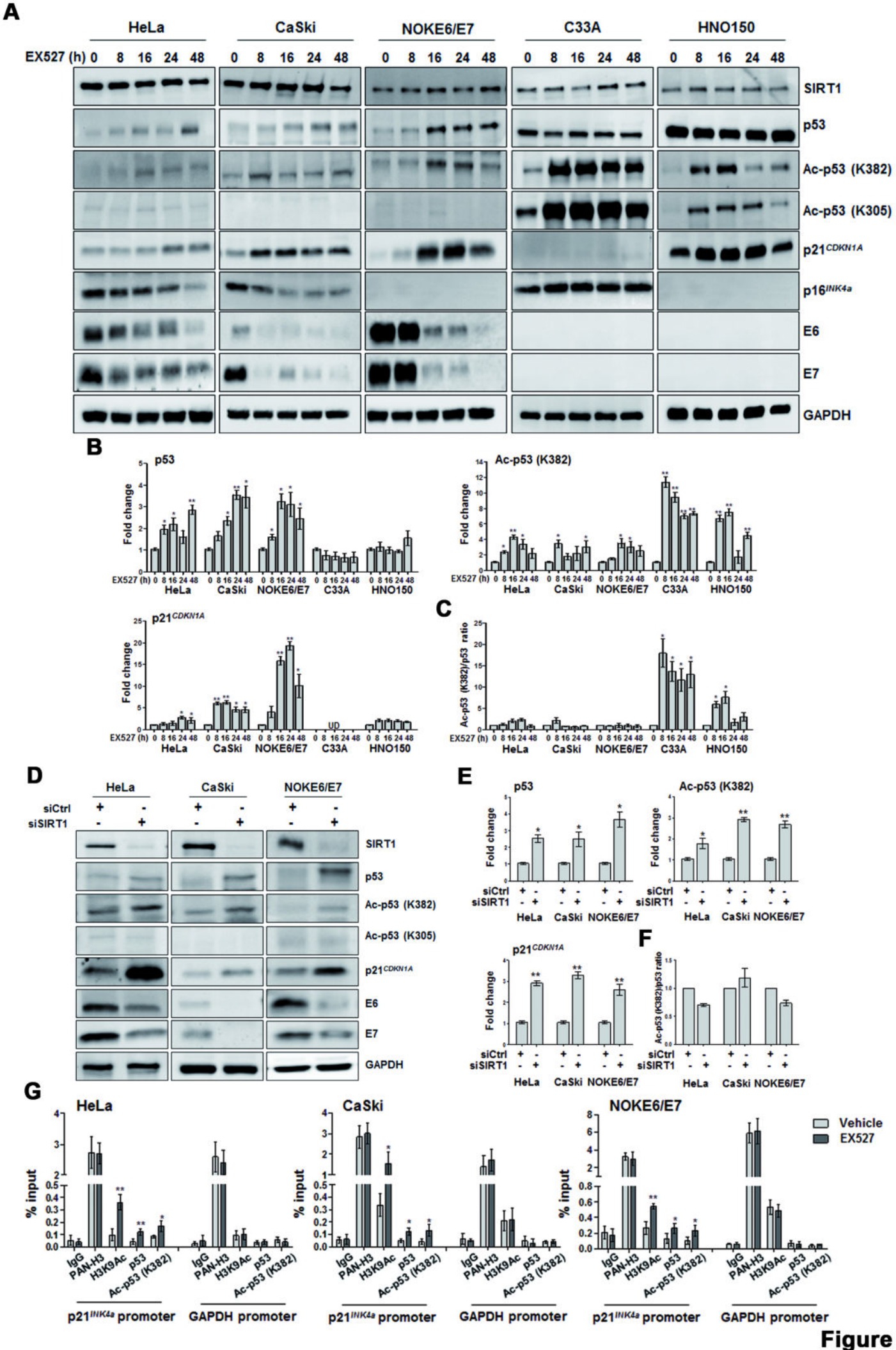
A
HeLa
CaSki
NOKE6/E7
C33A
HNO150
EX527 (h) 0 8 16 24 48
SIRT1
p53
Ac-p53 (K382)
Ac-p53 (K305)
p21CDKN1A
p16INK4a
E6
E7
GAPDH
B
p53
Ac-p53 (K382)
p21CDKN1A
Fold change
UD
C
Ac-p53 (K382)/p53 ratio
D
siCtrl
siSIRT1
E
F
G
% input
Vehicle
EX527
IgG
PAN-H3
H3K9Ac
p53
Ac-p53 (K382)
p21INK4a promoter
GAPDH promoter

Figure 2

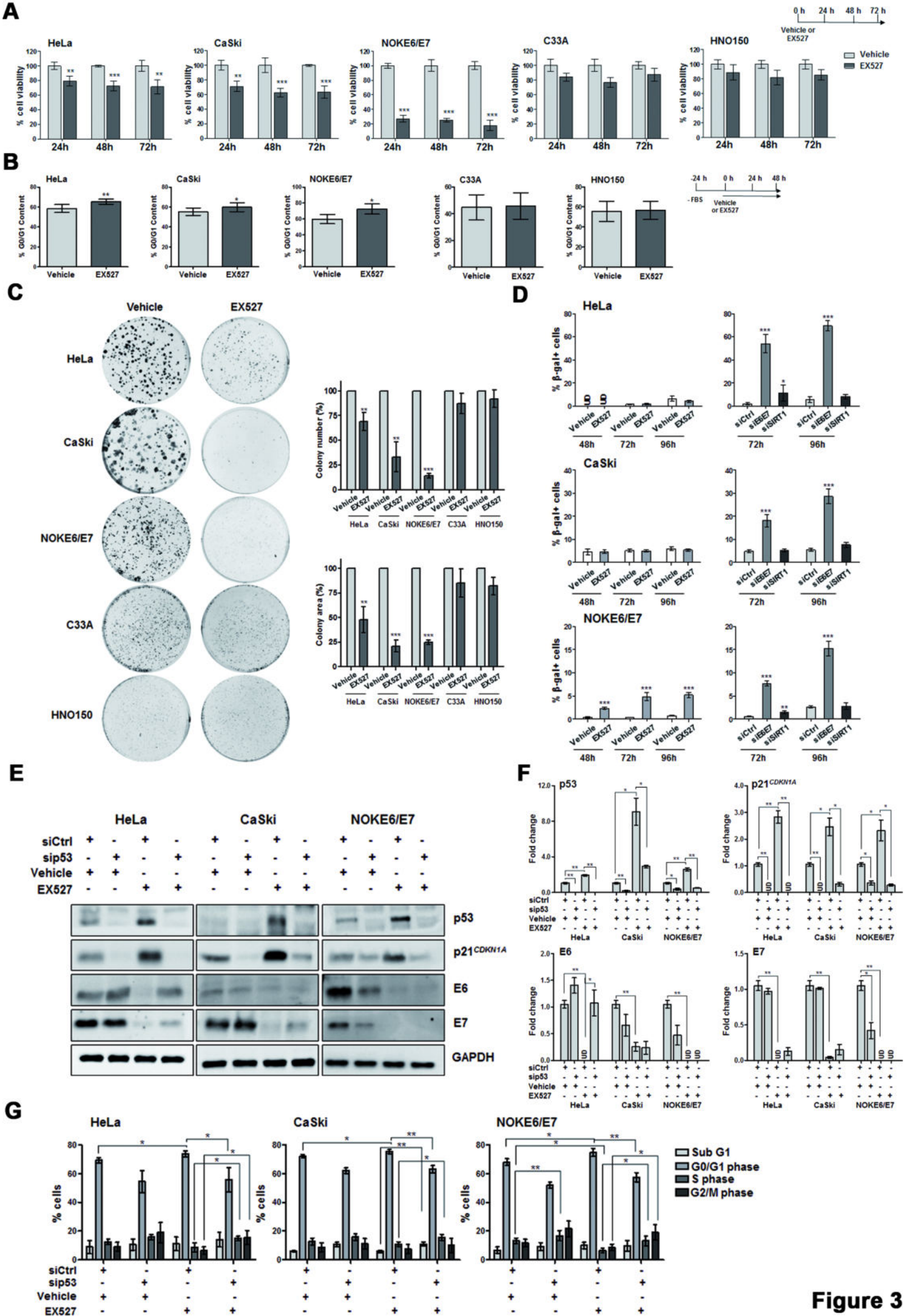
A
HeLa
CaSki
NOKE6/E7
C33A
HNO150
% cell viability
24h
48h
72h
0 h
24 h
48 h
72 h
Vehicle or EX527
Vehicle
EX527
B
% G0/G1 Content
-24 h
0 h
24 h
48 h
- FBS
Vehicle or EX527
C
Vehicle
EX527
Colony number (%)
Colony area (%)
D
% β-gal+ cells
siCtrl
siE6E7
siSIRT1
E
siCtrl
sip53
Vehicle
EX527
p53
p21CDKN1A
E6
E7
GAPDH
F
Fold change
UD
G
% cells
Sub G1
G0/G1 phase
S phase
G2/M phase

Figure 3

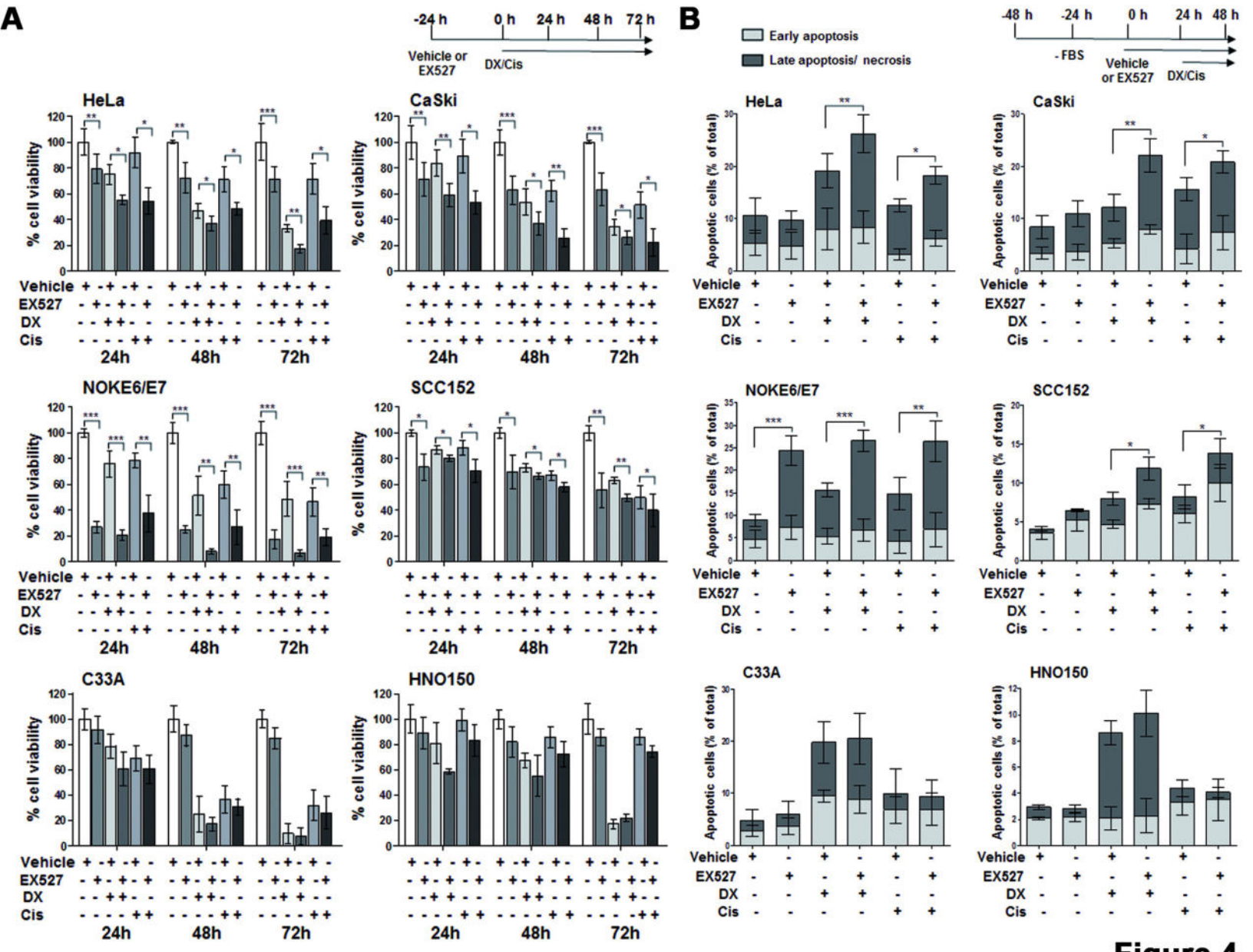
A
-24 h
0 h
24 h
48 h
72 h
Vehicle or EX527
DX/Cis
HeLa
CaSki
NOKE6/E7
SCC152
C33A
HNO150
% cell viability
Vehicle
EX527
DX
Cis
24h
48h
72h
B
Early apoptosis
Late apoptosis/ necrosis
-48 h
-24 h
0 h
24 h
48 h
- FBS
Vehicle or EX527
DX/Cis
Apoptotic cells (% of total)

Figure 4

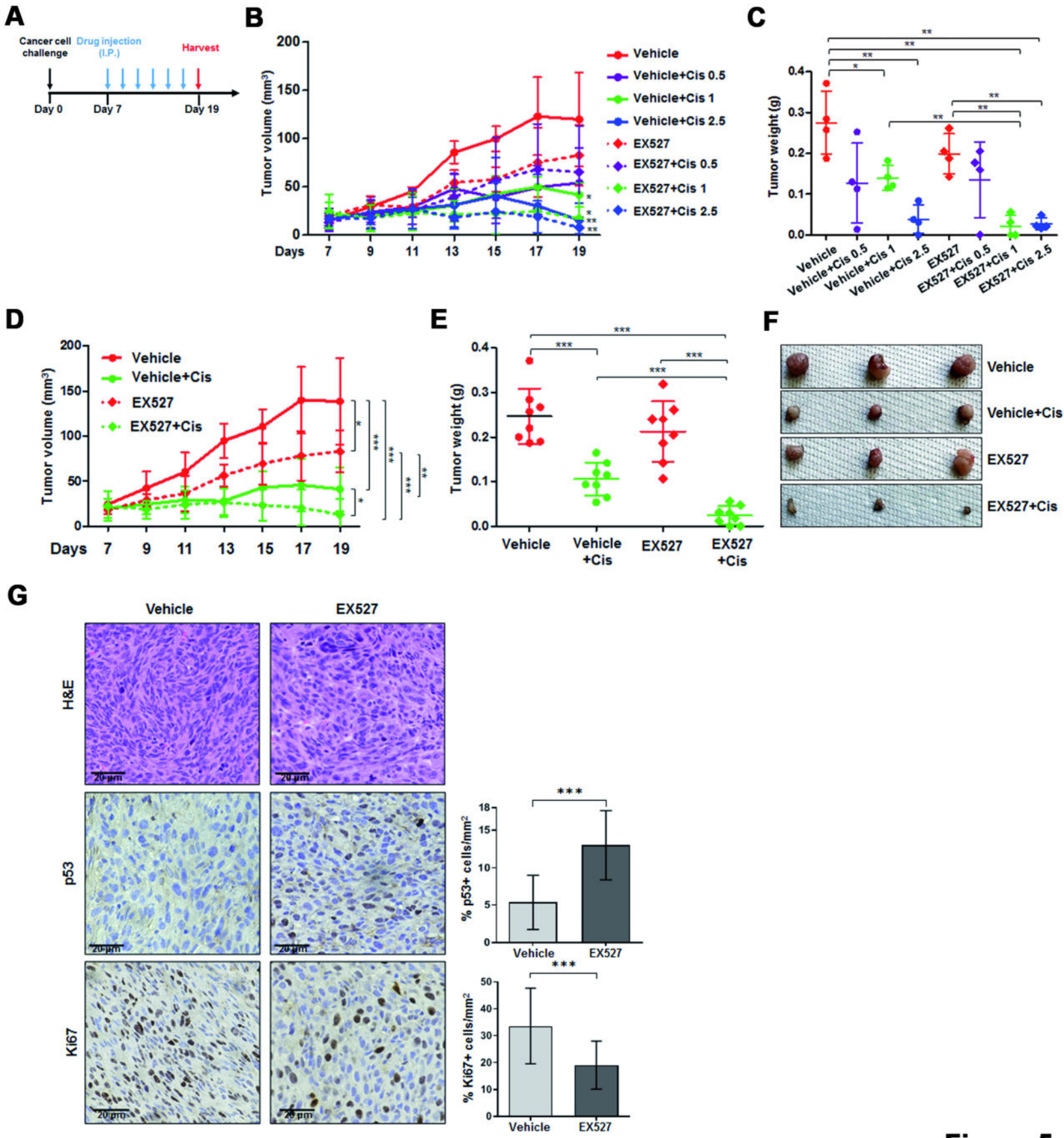
A
Cancer cell challenge
Drug injection (I.P.)
Harvest
Day 0
Day 7
Day 19
B
Tumor volume (mm³)
Days
Vehicle
Vehicle+Cis 0.5
Vehicle+Cis 1
Vehicle+Cis 2.5
EX527
EX527+Cis 0.5
EX527+Cis 1
EX527+Cis 2.5
C
Tumor weight (g)
Vehicle
Vehicle+Cis 0.5
Vehicle+Cis 1
Vehicle+Cis 2.5
EX527
EX527+Cis 0.5
EX527+Cis 1
EX527+Cis 2.5
D
Tumor volume (mm³)
Vehicle
Vehicle+Cis
EX527
EX527+Cis
Days
E
Tumor weight (g)
Vehicle
Vehicle +Cis
EX527
EX527 +Cis
F
Vehicle
Vehicle+Cis
EX527
EX527+Cis
G
Vehicle
EX527
H&E
p53
Ki67
20 μm
% p53+ cells/mm²
% Ki67+ cells/mm²
Vehicle
EX527

Figure 5

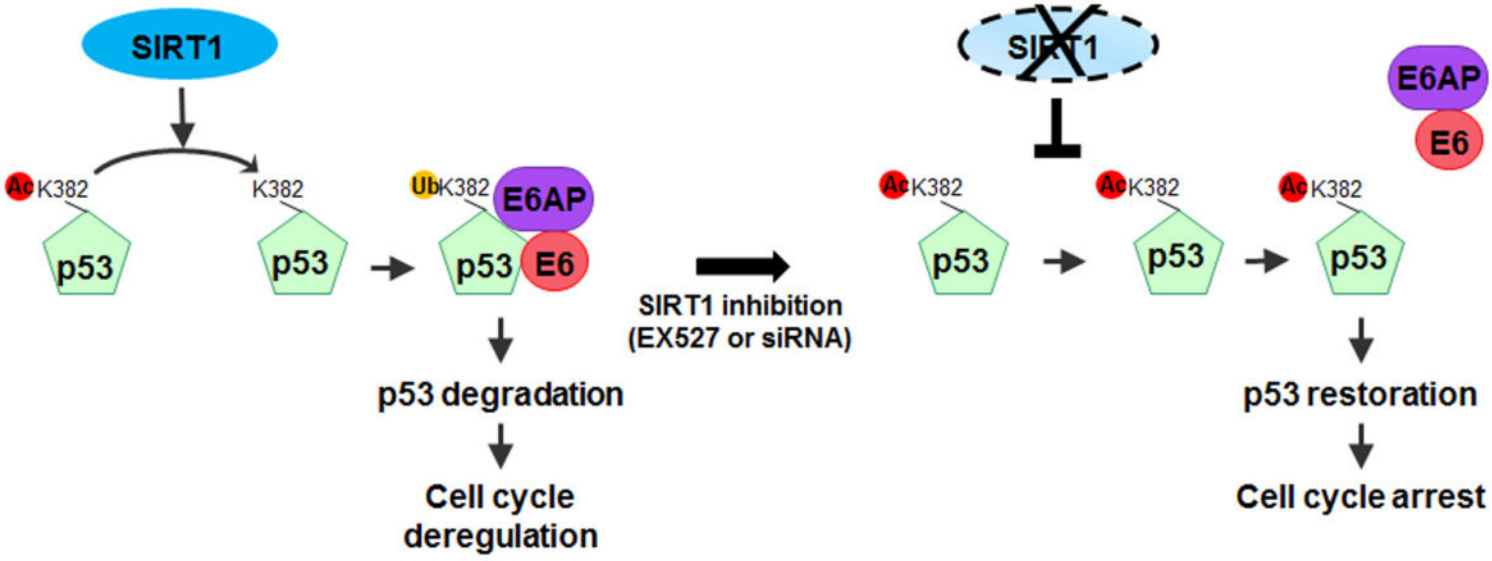
SIRT1
Ac K382
K382
p53
p53
Ub K382
E6AP
p53
E6
p53 degradation
Cell cycle deregulation
SIRT1 inhibition (EX527 or siRNA)
SIRT1
E6AP
E6
Ac K382
Ac K382
Ac K382
p53
p53
p53
p53 restoration
Cell cycle arrest

Figure 6